New Phytologist

Research

Mitochondrial phosphoenolpyruvate carboxylase contributes to carbon fixation in the diatom *Phaeodactylum tricornutum* at low inorganic carbon concentrations

Guilan Yu[1,4]*, Kensuke Nakajima[2], Ansgar Gruber[1,3], Carolina Rio Bartulos[1], Alexander F. Schober[1], Bernard Lepetit[1], Elizabeth Yohannes[1], Yusuke Matsuda[2] and Peter G. Kroth[1]*

[1]Fachbereich Biologie, Universität Konstanz, 78457, Konstanz, Germany; [2]Department of Bioscience, School of Biological and Environmental Sciences, 1 Gakuen Uegahara, Sanda, Hyogo 669-1330, Japan; [3]Institute of Parasitology, Biology Centre, Czech Academy of Sciences, 370 05, České Budějovice, Czech Republic; [4]Present address: School of Life Science, Key Laboratory of Aquatic Animal Resources and Utilization, Nanchang University, Nanchang, China

Authors for correspondence:
Guilan Yu
Email: yuguilan.1987@163.com

Peter G. Kroth
Email: peter.kroth@uni-konstanz.de

Received: *27 January 2022*
Accepted: *21 April 2022*

New Phytologist (2022) **235:** 1379–1393
doi: 10.1111/nph.18268

Key words: C_4 photosynthesis, carbon concentrating mechanism (CCM), diatoms, *Phaeodactylum tricornutum*, phosphoenolpyruvate carboxylases (PEPC), reverse genetics, TALEN.

Summary

- Photosynthetic carbon fixation is often limited by CO_2 availability, which led to the evolution of CO_2 concentrating mechanisms (CCMs). Some diatoms possess CCMs that employ biochemical fixation of bicarbonate, similar to C_4 plants, but whether biochemical CCMs are commonly found in diatoms is a subject of debate.
- In the diatom *Phaeodactylum tricornutum*, phosphoenolpyruvate carboxylase (PEPC) is present in two isoforms, PEPC1 in the plastids and PEPC2 in the mitochondria. We used real-time quantitative polymerase chain reaction, Western blots, and enzymatic assays to examine PEPC expression and PEPC activity, under low and high concentrations of dissolved inorganic carbon (DIC).
- We generated and analyzed individual knockout cell lines of PEPC1 and PEPC2, as well as a PEPC1/2 double-knockout strain. While we could not detect an altered phenotype in the PEPC1 knockout strains at ambient, low or high DIC concentrations, PEPC2 and the double-knockout strains grown under ambient air or lower DIC availability conditions showed reduced growth and photosynthetic affinity for DIC while behaving similarly to wild-type (WT) cells at high DIC concentrations. These mutants furthermore exhibited significantly lower $^{13}C/^{12}C$ ratios compared to the WT.
- Our data imply that in *P. tricornutum* at least parts of the CCM rely on biochemical bicarbonate fixation catalyzed by the mitochondrial PEPC2.

Introduction

Diatoms are an important part of the marine phytoplankton and are responsible for a significant portion of oceanic primary production (Nelson *et al.*, 1995; Falkowski & Raven, 1997). Photosynthesis is a fundamental process for primary productivity, and ribulose-1,5-biphosphate carboxylase/oxygenase (Rubisco) is the key enzyme for CO_2 fixation in the vast majority of oxygenic photosynthetic organisms, including photosynthetic Proteobacteria, and some Chloroflexi (Andersson & Backlund, 2008). Rubisco catalyzes the carboxylation reaction of ribulose-1,5-bisphosphate (RuBP), producing two molecules of the C_3 compound 3-phosphoglycerate, the primary product of carbon fixation in most photosynthetic organisms. However, the dissolved inorganic carbon (DIC) in seawater corresponds to a CO_2 concentration of 10–15 μM at pH 8.2 (Riebesell *et al.*, 1993), which is much lower than the value of the Michaelis–Menten constant (K_m = 20–60 μM) for CO_2 concentration in the proximity of the diatom Rubisco enzyme (Badger *et al.*, 1998; Whitney *et al.*, 2011; Young *et al.*, 2016). To circumvent CO_2 limitation, diatoms, as well as many other phytoplankton, use CO_2 concentrating mechanisms (CCMs) that comprise the active uptake and transport of inorganic carbon to increase the CO_2 concentration in the proximity of Rubisco, improving photosynthetic efficiency, especially in a carbon-limited environment (Kaplan & Reinhold, 1999; Burkhardt *et al.*, 2001; Matsuda *et al.*, 2001, 2017; Giordano *et al.*, 2005; Reinfelder, 2010; Hopkinson *et al.*, 2011; Kikutani *et al.*, 2016; Clement *et al.*, 2017; Shen *et al.*, 2017; Jensen *et al.*, 2019; Launay *et al.*, 2020). There are also phytoplankton that lack CCMs (e.g. Chrysophytes (Maberly *et al.*, 2009)).

Two types of CCM can be distinguished: biophysical and biochemical. Biophysical CCMs include the active transport of bicarbonate (HCO_3^-) across biological membranes, coupled with facilitated conversion between CO_2 and bicarbonate. In biochemical CCMs, C_3 compounds are carboxylated by phosphoenolpyruvate carboxylases (PEPCs), leading to the formation of C_4 acids (C_4 photosynthesis). One crucial point here is that the

substrate for PEPCs is not CO_2 but HCO_3^-, which is more abundant in the ocean waters. The C_4 compounds in eukaryotic photoautotrophs can then be transported to the cytosol, mitochondria, or chloroplasts, where they are eventually decarboxylated by a decarboxylase to release CO_2 in close proximity to Rubisco, at either the cellular or organellar level (Sage, 2004). In most C_4 plants, the reactions of C_4 photosynthesis are spatially separated by cell differentiation (Kranz-type anatomy) (Sage *et al.*, 2012). In several terrestrial and aquatic plants, and in a few algae, single-cell biochemical CCMs have also been observed (Salvucci & Bowes, 1981; Ascencio & Bowes, 1983; Reiskind & Bowes, 1991; Magnin *et al.*, 1997; Lara *et al.*, 2002; Voznesenskaya *et al.*, 2002; Edwards *et al.*, 2004; Zhang *et al.*, 2014).

In diatoms, the essential components involved in biophysical CCMs include HCO_3^- transporters (Rotatore *et al.*, 1995; Burkhardt *et al.*, 2001; Nakajima *et al.*, 2013) and carbonic anhydrases (CAs) (Morel *et al.*, 1994, 2002; Colman & Rotatore, 1995; Burkhardt *et al.*, 2001; Hopkinson *et al.*, 2013; Kikutani *et al.*, 2016); some of the latter have recently been shown to be extracellular (Tsuji *et al.*, 2021). Some CAs also have been shown to reside, together with Rubisco, in the pyrenoid (Kikutani *et al.*, 2016). A number of studies greatly improved our understanding of these biophysical CCMs (Hopkinson *et al.*, 2011; Nakajima *et al.*, 2013; Clement *et al.*, 2017; Matsuda *et al.*, 2017; Shen *et al.*, 2017; Young & Hopkinson, 2017; Jensen *et al.*, 2019).

As far as biochemical CCMs are concerned, the findings in diatoms are far from clear. Observations of principal ^{14}C-labelled intracellular C_4 compounds (malate), ^{14}C transfer from malate to 3-phosphoglyceric acid (PGA) and sugar in CO_2-limited cells, and the high activity of phosphoenolpyruvate carboxylase (PEPC) at low CO_2 concentrations, indicate the existence of a biochemical CCM in the marine diatom *Thalassiosira weissflogii* (Reinfelder *et al.*, 2000). Some biochemical and molecular data also suggest a C_4-assisted photosynthesis in other diatoms, such as *Thalassiosira pseudonana* and *Phaeodactylum tricornutum*. Beardall *et al.* (1976) showed predominantly early labeling of C_4 compounds in *P. tricornutum*, suggesting a C_4 pathway. A two- to four-fold greater transcript abundance of two *PEPCs* was detected in *T. pseudonana* under low CO_2 growth conditions (McGinn & Morel, 2008), as well as an increase in the abundance of *PEPC* transcripts when cells were shifted from high to low CO_2 conditions (Kustka *et al.*, 2014). Other experimental evidence argues against the presence of biochemical CCMs in diatoms: pyruvate, orthophosphate dikinase (PPDK) silencing experiments via RNAi (Haimovich-Dayan *et al.*, 2013) and isotope labeling experiments (Roberts *et al.*, 2007) did not support the presence of a C_4 CCM in *P. tricornutum* or *T. pseudonana*, respectively. Lastly, a recent study suggested that a C_4 CCM is absent in all of the examined diatom species, including *T. weissflogii*, and that diatom CCMs rely mostly on HCO_3^- transporters and CAs (Clement *et al.*, 2017).

Genomic analyses of *T. pseudonana* (Armbrust *et al.*, 2004) and *P. tricornutum* (Bowler *et al.*, 2008) revealed that genes required for the C_4 pathways exist in both diatom species (Kroth *et al.*, 2008). Localization experiments with GFP fusion proteins in *T. pseudonana* and in *P. tricornutum* suggest that two carboxylating enzymes, PEPC1 and PEPC2, are located in the matrix of the periplastidic compartment and the mitochondria, respectively (Tanaka *et al.*, 2014; Ewe *et al.*, 2018). The periplastidic space in diatoms between the second and the third of the four plastid envelope membranes is considered to represent the former cytosol of the secondary red algal endosymbiont (Kroth, 2002). Potential decarboxylation enzymes, like the NAD-dependent malic enzyme (NAD-ME) and the phosphoenolpyruvate carboxykinase (PEPCK), are located in the cytosol and mitochondria, respectively, in *T. pseudonana* and in *P. tricornutum* (Tanaka *et al.*, 2014; Ewe *et al.*, 2018). None of the decarboxylases so far identified in diatoms has yet been found to be located in the plastid stroma of these two diatom species, while other enzymes have been suggested to be potentially involved in decarboxylation (Kustka *et al.*, 2014).

In order to understand the origin and the role of PEPC1 and PEPC2 in diatoms, we used reverse genetics to generate knockout individual and simultaneous genes of the two *PEPCs* in *P. tricornutum* and studied them comprehensively via molecular, biochemical and physiological approaches.

Materials and Methods

Strains and culture conditions

The marine diatom *Phaeodactylum tricornutum* Bohlin strain UTEX 646, obtained from Culture Collection of Algae, University of Texas (https://utex.org/) was grown in f/2 medium with artificial half-concentrated sea salts (16.6 g l^{-1}, Tropic Marin; Dr Biener GmbH, Leubsdorf, Germany) and other supplements (Guillard & Ryther, 1962; Guillard, 1975). Solid f/2 media contained 12 g l^{-1} Bacto Agar (Becton, Dickinson & Co., Le Pont de Claix, France). Cells were grown at 20°C, and illuminated with a light intensity of 65–70 µmol photons m^{-2} s^{-1} (16 h : 8 h, light : dark photocycle). The cultures inoculated from the exponential phase cultures were grown under either low CO_2 (0.01 vol% = LC), pseudo ambient CO_2 (0.04 vol% = AC), high CO_2 (0.6 vol% = HC), or ultra-high CO_2 (1 vol% = UHC). Cultivation occurred in two-tier culture vessels (Yu *et al.*, 2017) or under ambient air in Erlenmeyer flasks on a horizontal shaker. The cultures used for DIC-dependent O_2 evolution experiments were grown under continuous illumination (50–75 µmol photons m^{-2} s^{-1}) at 20°C under constant aeration with 1 vol% CO_2 or ambient air.

Purification of recombinant phosphoenolpyruvate carboxylase and enzymatic assays

The sequences of two *PEPC* genes (JGI protein IDs – PEPC1, 56026; PEPC2, 20853) which encode the mature PEPC proteins were cloned from *P. tricornutum* genomic DNA into overexpression vector pET28a(+) (Novagen/Merck KGaA, Darmstadt, Germany). The resulting vectors pET28a-His-PEPC1 and pET28a-His-PEPC2 were used for genetic transformation of *Escherichia coli* BL21 (DE3 Rosetta, Novagen) by electroporation

(MicroPulser™; Bio-Rad, Feldkirchen, Germany). Single colonies were cultivated in LB medium at 37°C until an optical density at 600 nm (OD_{600}) of 0.5–0.6 was reached. Thereafter, gene expression was induced with isopropyl-β-D-1-thiogalactopyranoside (IPTG) (Carl Roth, Karlsruhe, Germany) at a final concentration of 0.5 mM, and the cultures were incubated at 20°C overnight in a rotary shaker. The control cells were not treated with IPTG, but were otherwise cultured under the same conditions. Next, 2 ml *E. coli* cells from 1 l of IPTG induced culture were harvested by centrifugation at 5000 ***g*** for 3 min and analyzed by sodium dodecyl sulfate–polyacrylamide gel electrophoresis (SDS-PAGE). The residual *E. coli* cultures were harvested and resuspended in lysis buffer (50 mM Hepes-NaOH pH 8.0, 100 mM NaCl, 25 mM imidazole, and proteinase inhibitor). Cells were disrupted with a French press (FA-079; SLM Aminco) at a pressure of *c.* 6.89 MPa (1000 psi on the instrument scale), twice, at 4°C. The cell lysate was centrifuged at maximum speed (16 000 ***g***) for 30 min at 4°C. The supernatant was passed through 0.22 µm filters to remove larger particles, and then applied to a His Trap FF crude column (GE Healthcare, Uppsala, Sweden) using an ÄKTA Fast Protein Liquid Chromatography (FPLC) system (P900; Amersham Biosciences). The flow through was collected by applying a constant flow of 5% filtered B1 buffer (50 mM Hepes-NaOH pH 8.0, 100 mM NaCl, 500 mM imidazole) and 95% filtered A1 buffer (50 mM Hepes-NaOH pH 8.0, 100 mM NaCl). Subsequently, the His tag-PEPC fusion proteins were eluted with a gradient elution buffer (5% B1 to 100% B1). Based on the elution profile analysed by SDS-PAGE, protein purification occurred at *c.* 50% B1. For enzymatic assays, 1 µg of purified recombinant PEPC protein was used for each assay in 1 ml reaction volume. For PEP or HCO_3^- saturation curves, increasing PEP or HCO_3^- concentrations were added to the reaction volume, while the other substrates and malate dehydrogenase (MDH) were present in excess. The obtained kinetic data were plotted and analyzed using nonlinear regression in SIGMAPLOT (v.12.5). Data obtained at various substrate concentrations were fitted to the Michaelis–Menten equation (Michaelis & Menten, 1913) for hyperbolic kinetics and to the Hill equation (Hill, 1910) for sigmoidal kinetics.

Construction of PEPC TALEN knockout vectors, the nuclear transformation of *Phaeodactylum tricornutum* and the selection of transformants

Potential TALEN target sites for the *PEPC1* and *PEPC2* genes were generated using the TAL EFFECTOR NUCLEOTIDE TARGETER v.2.0 software (Doyle *et al.*, 2012). The target sites for both *PEPCs* located in the exon region of the functional domain were chosen according to the parameters described in Serif *et al.* (2017), excluding those sites with potential off-target effects. *PEPC* TALEN knockout vectors were generated as previously described (Sanjana *et al.*, 2012; Serif *et al.*, 2017). The *PEPC* TALEN plasmids were assembled using primers BL25_Hex-F and BL26_Hex-R (Supporting Information Table S1), and the resulting plasmids were digested with the restriction enzyme AfeI and then sequenced (GATC-Eurofins, Konstanz, Germany) with primers BL27_TALE-Seq-F1, BL28_TALE-Seq-F2 and BL29_TALE-Seq-R1 (Table S1) to verify that the integration and orientation were correct.

In order to generate PEPC1 and PEPC2 knockout mutants, *P. tricornutum* was genetically transformed with a mixture of the two *PEPC* TALEN upstream and downstream plasmids (5 µg each) using the Biolistic PDS-1000/He Particle Delivery System (Bio-Rad) as described previously (Zaslavskaia *et al.*, 2000). Five micrograms of each TALEN plasmid (i.e. four plasmids, combining two TALEN pairs) were used to generate PEPC double-knockout mutants by simultaneous transformation. The transformed cells were plated onto the f/2 media plates containing 75 µg ml^{-1} Zeocin (Invitrogen) and 150 µg ml^{-1} Nourseothricin (ClonNat; Werner Bioagents, Jena, Germany) for resistance selection.

Genotype characterization of PEPC transformants

The molecular methods applied to characterize the cell lines resulting from genetic transformation with the TALEN constructs, including DNA extraction, allele-specific polymerase chain reaction (PCR), sequencing, Southern blots, and Western blots are described in the Methods S1.

Quantitative real-time polymerase chain reaction

Wild-type (WT) *P. tricornutum* cells were harvested in the exponential phase, grown under LC and HC conditions (see 'Strains and culture conditions' in the Materials and Methods section). RNA was extracted using RNAPure and a Total RNA Kit (peqGOLD; VWR, Leuven, Belgium). Residual genomic DNA was digested using a DNase Digest Kit (peqGOLD; VWR) during RNA extraction. Ribosomal ribonucleic acid *18S* (Ensembl Gen ID: EPrPhatr3G00000013183) was used as the reference gene, which is stably transcribed under LC and HC conditions. The real-time polymerase chain reaction (RT-PCR) was performed on an Applied Biosystems™ 7500 Fast Real-Time PCR System (Thermo Fisher Scientific, Freiburg, Germany) under the following PCR conditions: denaturation at 95°C for 20 s, followed by 40 cycles of denaturation at 95°C for 3 s, then annealing and elongation at 57°C for 30 s as described by Lepetit *et al.* (2013). The primers used here are listed in Table S1. Cycle threshold values and relative transcript levels were analyzed using the online software REAL-TIME PCR MINER v.3.0 (Zhao & Fernald, 2005; Lepetit *et al.*, 2013).

Measurement of PEPC activity

A total of 2×10^9 *P. tricornutum* cells in the exponential phase were centrifuged (Sorvall RC 6 Plus centrifuge; Fisher Scientific, Schwerte, Germany) for PEPC activity measurement. The pellet was washed with 10 ml of protein lysis buffer (50 mM Tris–HCl, pH 8.0, 0.1 mM EDTA, 15 mM $MgCl_2$, 10 vol% glycerol) and harvested by another centrifugation, and the resulting pellet was resuspended in 2.5 ml protein lysis buffer and 140 µl 1× EDTA-free Protease Inhibitor Cocktail (Roche). The sample

was then passed three times through a French press (FA-079; SLM Aminco) at a pressure of 1000 psi (*c.* 6.89 MPa) in a cooled mini-cell and centrifuged twice (Optima-max; Beckman Coulter, Krefeld, Germany). Next, 2 ml of the resulting supernatant was cleaned up using a PD-10 desalting column (GE Healthcare, Solingen, Germany) according to the manufacturer's protocol. The protein concentration of the desalted protein extract was determined via a Bradford assay (Bradford, 1976). For the measurement of PEPC activity, enzymatic buffer (50 mM Tris–HCl, pH 8.5, 0.1 mM EDTA, 15 mM $MgCl_2$, 10 vol% glycerol) was added to a 1-cm diameter cuvette (quartz; Neolab, Heidelberg, Germany), followed by the addition of 20 mM HCO_3^-, 25 units of MDH (Carl Roth), 0.1 mM NADH (Carl Roth) and 100 µg desalted protein extract. The PEPC reaction was initiated by the addition of 15 mM PEP (AppliChem GmbH, Darmstadt, Germany), to a total volume of 1 ml. Enzymatic activity was continuously followed by recording the absorbance of NADH at 340 nm with a photometer (Ultrospec™ 8000; GE Healthcare) according to the manufacturer's instructions.

Determination of photosynthetic parameters

Chl *a* determination Two hundred microlitres of DIC-free f/2 medium washed cells were centrifuged at 16 000 ***g***. Next, 100 µl dimethyl sulfoxide (DMSO) was added to the pellet and vortexed at maximum speed. Afterwards, 0.9 ml of methanol was added and the tube was mixed again at maximum speed. After centrifugation at 16 000 ***g*** for 2 min, the supernatant was used for Chl *a* measurement in a spectrophotometer (UH5300; Hitachi High-Tech Science Co., Tokyo, Japan). Chl *a* concentrations were calculated as described previously (Jeffrey & Humphrey, 1975).

Dissolved inorganic carbon concentration-dependent O_2 evolution *Phaeodactylum tricornutum* WT and mutant cultures (60 ml) from the mid-logarithmic phase (OD_{730} = 0.2–0.4) were harvested by centrifugation at 2000 ***g*** for 3 min at room temperature (KN-70; Kubota Co., Tokyo, Japan). Cell pellets from the LC and UHC growth conditions were washed with DIC-free f/2 medium buffered with 10 mM Tris–HCl (pH 8.2) three and five times, respectively. Cells were then suspended in the DIC-free f/2 medium at a Chl *a* concentration of 10 µg ml^{-1}. The rate of photosynthetic O_2 evolution at various DIC concentrations was measured with a Clark-type oxygen electrode (Hansatech Instruments Ltd, Norfolk, UK) (Matsuda *et al.*, 2001). Cells were exposed to 150 µmol photons m^{-2} s^{-1} until the CO_2 compensation point (the DIC concentration at which no net consumption of O_2 was measured) was reached. Then, the DIC concentration at the CO_2 compensation point was measured with a gas chromatograph (GC) (GC-8A; Shimadzu Co., Kyoto, Japan) equipped with a methanizer and a flame ionization detector (GC-FID; Birmingham & Colman, 1979). Afterwards, the light intensity was increased to 300 µmol photons m^{-2} s^{-1} and various concentrations of DIC were added to measure P_{max} and $K_{0.5}$ [DIC]. $K_{0.5}$ [DIC] values were determined by rectangular-hyperbola data fitting with nonlinear least squares regression.

Maximum photosynthetic efficiency of photosystem II (F_v/F_m) *Phaeodactylum tricornutum* culture in the mid-logarithmic phase with 1 µg ml^{-1} Chl *a* was used for F_v/F_m measurements using an AquaPen-C AP 100 (Photon Systems Instruments, Drásov, Czech Republic). F_v/F_m was measured and calculated as described previously (Huang *et al.*, 2018).

Stable isotope analyses

Wild-type and PEPC knockout mutants of *P. tricornutum* grown under LC, AC, and HC conditions as described by Yu *et al.* (2017) were harvested by centrifugation (Allegra 25R Centrifuge; Beckman Coulter). The pellets were immediately frozen in liquid nitrogen and afterwards were freeze-dried overnight (Christ Alpha 1–4; B. Braun Biotech International, Melsungen, Germany). Dried samples of *c.* 0.3 mg (dry weight) were then pre-weighed in tin cups and combusted using the vario Microcube elemental analyser (Elementar Analysensysteme GmbH, Langenselbold, Germany); the resultant CO_2 gas was introduced into a Micromass Isoprime isotope ratio mass spectrometer (Isoprime, Cheadle, UK) via a continuous flow-through inlet system. Ratios of $^{13}C/^{12}C$ for each sample are expressed in the delta ($\delta^{13}C$) notation in parts per million (‰). These values are relative to the Vienna Pee Dee Belemnite (VPDB) standard for carbon.

We obtained stable isotope ratios by using the following equation:

$$\delta^{13}C\ (‰) = 1000 \times \left(R_{sample}/R_{standard} - 1\right)$$

where R is $^{13}C/^{12}C$. Internal laboratory standards indicate that our measurement errors (SD) were ± 0.05%.

The salts used for the preparation of f/2 medium and the $KHCO_3/K_2CO_3$ powders were also weighed into capsules to determine the background $\delta^{13}C$ (Table S2).

Statistical analysis

Data are given as arithmetic means with SDs. Student's *t*-test was applied using the SIGMAPLOT v.12.5 software package to evaluate the difference between mean values. The phylogenetic analysis of the PEPC method is described in Methods S1.

Results

Phylogenetic distribution of *PEPC* genes

Phosphoenolpyruvate carboxylase proteins are present in all investigated groups, including photosynthetic eukaryotes, various eubacteria, and archaea. While most algal organisms have just one copy of a PEPC, both a 'housekeeping' (anaplerotic) and a 'photosynthetic' PEPC are widespread in the biochemical CCMs of flowering plants, including the aquatic facultative C_4 plant *Hydrilla verticillata* in which the C_4 and the Calvin pathways co-exist in the same cell (Besnard *et al.*, 2003; Rao *et al.*, 2008).

Comparing different PEPC sequences via phylogenetic analyses reveals that a gene duplication of the PEPCs apparently occurred specifically within the group of diatoms (Fig. S1), as two copies can be found in all studied diatoms. The diatom sequences are furthermore clearly separated from the PEPC sequences of brown algae that apparently only possess a single *PEPC* gene. In order to reveal potentially different functions of the two diatom PEPCs, we have studied the purified recombinant enzymes as well as *P. tricornutum* PEPC knockout mutants.

Kinetic differences between the two recombinant PEPCs

As a prerequisite for biochemical analyses, we expressed the two *P. tricornutum* PEPCs in *E. coli* as mature proteins with added His tags and without the predicted cleavable N-terminal presequences. The proteins were purified from crude *E. coli* extracts using a Ni-NTA column (Fig. 1a,b). The specific activities of the enzymes (PEPC1: 41 μM min^{-1} mg^{-1} and PEPC2: 68 μM min^{-1} mg^{-1}) were in a similar range as those reported in a previous study on *P. tricornutum* PEPC2 (Chang *et al.*, 2014; named PEPC1 therein). To investigate the affinities of recombinant PEPC proteins for the substrates PEP and HCO_3^-, PEPC activity was measured at different PEP or HCO_3^- concentrations. The PEP saturation curves of both PEPCs are shown in Fig. 1(c). Both proteins show a sigmoidal saturation curve for the substrate PEP, which indicates cooperative PEP binding. The respective calculated K_m values of PEPC1/2 for PEP are 1 mM/1.6 mM, respectively, indicating that the affinity of PEPC1 for PEP is higher than that of PEPC2 (Table S3). The HCO_3^- saturation curves of both PEPCs are hyperbolic in form (Fig. 1d). The respective K_m values of PEPC1/2 for HCO_3^- are 0.85 mM/0.11 mM, indicating that the affinity of PEPC1 for HCO_3^- is about 8 times lower than the affinity of PEPC2 for HCO_3^- (Table S4).

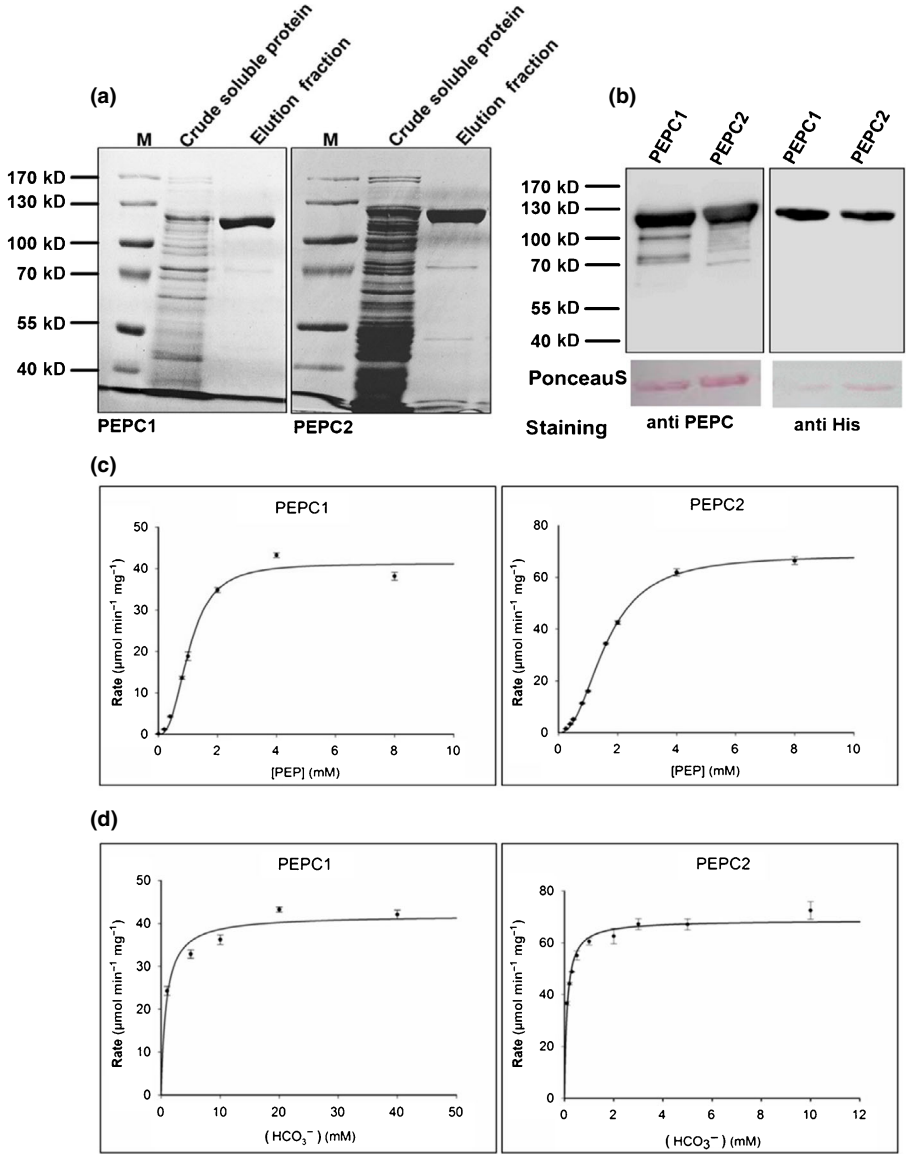

Fig. 1 Biochemical properties of the recombinant *Phaeodactylum tricornutum* PEPC1 and PEPC2 proteins. (a) Overexpression of recombinant PEPC1 and PEPC2 proteins and purification by His Trap chromatography. The crude soluble proteins and the elution fraction were both separated using sodium dodecyl sulfate–polyacrylamide gel electrophoresis (SDS-PAGE) and stained with Coomassie blue. M, protein marker. (b) The purified recombinant PEPC1 and PEPC2 proteins were incubated with a PEPC- and a His tag-directed antiserum, respectively. The membrane was stained with Ponceau S after blotting to show that an equal amount of PEPC protein was loaded for Western blots. (c) The saturation curve of recombinant phosphoenolpyruvate carboxylases (PEPCs) vs phosphoenolpyruvate (PEP), plotted according to the Hill equation. The error bars indicate the SDs of at least three independent biological replicates. (d) The saturation curve of recombinant PEPCs vs bicarbonate (HCO_3^-) was plotted according to the Michaelis–Menten equation. The error bars indicate SDs of at least three independent biological replicates.

Lastly, PEPC2 showed a higher maximum activity under the optimal conditions (Tables S3, S4).

CO_2-dependent regulation of PEPC mRNA, protein and enzymatic activity in *Phaeodactylum tricornutum*

In order to investigate a putative influence of CO_2 concentrations on the regulation of the two isoenzymes in *P. tricornutum*, we incubated WT cells at LC (0.01 vol%) and HC (0.6 vol%) CO_2 concentrations. Interestingly, the relative amounts of *PEPC1* and *PEPC2* transcripts did not change significantly between LC and HC (Fig. 2a). To investigate whether this result is reflected by the amount of PEPC protein, we quantified the levels of PEPC proteins under both LC and HC conditions. As attempts to obtain antisera specifically reacting with PEPC1 and PEPC2 failed, we used a commercially available polyclonal PEPC antiserum against plant PEPCs, which binds to both diatom proteins, PEPC1 and PEPC2 (Fig. 2b). As both isoforms show a similar size in SDS-PAGE analyses, we could only use this antiserum to estimate the total amounts of the PEPCs. The respective Western blots showed that total PEPC protein amounts did not change noticeably between the LC and HC conditions in WT cells (Fig. 2b). As shown in Fig. 2(c), we furthermore could not detect a significant difference in PEPC enzyme activity under LC and HC conditions. In order to characterize the general response of *P. tricornutum* to different CO_2 concentrations during culturing, we determined the relative transcript amounts of the HCO_3^- transporters SLC4-1, SLC4-2, and SLC4-4, which are involved in the biophysical CCM. As shown in Fig. S2, the *SLC4-1*, *SLC4-2*, and *SLC4-4* genes are much more highly expressed under LC than under HC conditions.

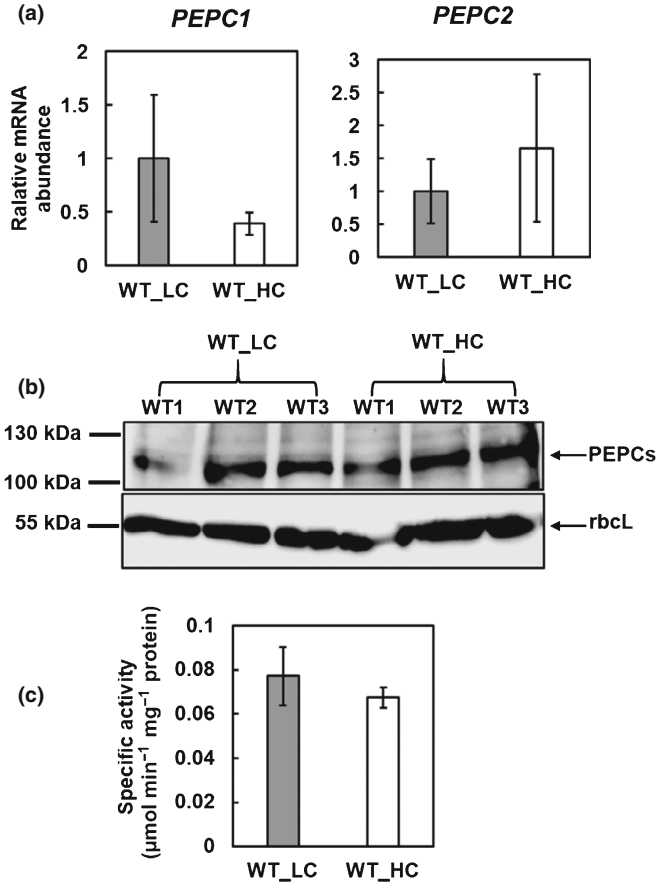

Fig. 2 Expression of PEPC1 and PEPC2 in *Phaeodactylum tricornutum* cells cultured under 0.01 vol% CO_2 (low CO_2; LC) and 0.6 vol% CO_2 (high CO_2; HC) under a 16 h : 8 h, light : dark photocycle. (a) Quantitative real-time polymerase chain reaction analysis of changes in *PEPC* transcript levels in response to cultivation under LC and HC conditions. Relative *PEPC* transcript levels with reference to 18S gene expression were normalized to the expression under LC conditions. The error bars indicate SDs of three independent replicate experiments. (b) Western blot analysis of phosphoenolpyruvate carboxylase (PEPC) protein expression under LC and HC conditions. Total soluble protein was extracted from wild-type (WT) cells, separated via sodium dodecyl sulfate–polyacrylamide gel electrophoresis (SDS-PAGE), blotted, and incubated with antiserum against PEPC that recognizes both PEPC isoforms. Antiserum-based detection of rbcL (ribulose bisphosphate carboxylase large chain) protein was used to verify identical loading. Three independent WT replicates were used for Western blotting under each CO_2 condition. (c) The specific enzymatic activity of PEPC in cellular extracts under LC and HC conditions. The error bars indicate SDs of at least three independent biological replicates.

Generation and screening of PEPC knockout transformants in *Phaeodactylum tricornutum*

To further investigate the function of the PEPCs, we knocked out the *PEPC1* and *PEPC2* genes in *P. tricornutum* both individually and simultaneously via a TALEN-based approach. In total, 38 PEPC1 knockout transformants, 23 PEPC2 knockout transformants, and 23 PEPC1/PEPC2 double-knockout transformants were collected after biolistic transformation. A detailed description of the mutant line characterization, including verification of a full knockout of both alleles is given in the Supporting Information (see 'Generation and screening of PEPC knockout transformants in *P. tricornutum*' in Methods S1; Table S5; Figs S3–S15). The strains that were finally selected for further characterization were PEPC1-23, -26, and -37; PEPC2-6, -13; and the double knockout strain PEPC1/2-7.

Protein expression and enzymatic activity of PEPC in PEPC knockout mutants

We studied the PEPC protein levels in the PEPC knockout mutants during the exponential growth phase using Western blots with a commercial antiserum that detects both PEPCs (with RbcL antiserum as a loading control). We could not detect any PEPC protein in the PEPC1/PEPC2 double-knockout strain PEPC1/2-7 (Fig. 3a), while the total amount of PEPC protein was partially reduced in the PEPC1 knockout lines 23, 26, and 37 (resulting from residual PEPC2 expression). Similarly, we also detected PEPC protein in the PEPC2 knockout lines 6 and 13 (Fig. 3a), resulting from PEPC1 expression. We furthermore tested PEPC enzyme activity in protein extracts of the wild-type and PEPC knockout mutants. PEPC1 knockout mutants show a similar total enzymatic activity as WT cells, while in PEPC2 knockout mutants PEPC activity is reduced by *c.* 60% compared

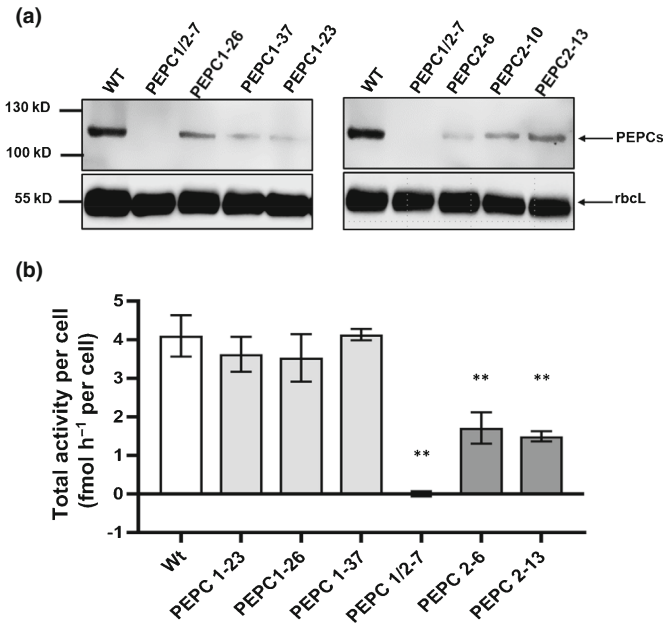

Fig. 3 Western blot analysis of the PEPC protein and PEPC enzymatic activity of wild-type (WT) and PEPC knockout mutants of *Phaeodactylum tricornutum*. (a) Western blot analysis of PEPC knockout lines and WT. Total soluble protein was extracted from selected lines, separated by sodium dodecyl sulfate–polyacrylamide gel electrophoresis (SDS-PAGE), blotted and incubated with antisera to *P. tricornutum* PEPC. Ribulose bisphosphate carboxylase large chain protein was detected as a loading control. (b) The PEPC enzymatic activity of WT and PEPC knockout mutants. The error bars indicate SDs of at least three independent biological replicates. Student's *t*-test was used to calculate the differences between WT and PEPC knockout mutants (**, $P < 0.01$).

to WT. In the PEPC1/PEPC2 double-knockout mutant we could not detect any PEPC activity (Fig. 3b). The characterization of PEPC knockout mutants by allele-specific PCR, sequencing, Southern blot, Western blot, and PEPC enzymatic activity measurements are summarized in Table S5.

Growth and F_v/F_m values of PEPC2 and PEPC1/PEPC2 double-knockout mutants under ambient air

Growth characteristics of the PEPC1, PEPC2, and PEPC1/2 knockout lines were determined under two different CO_2 conditions. The cells were cultured under AC (0.04 vol% CO_2) and HC (0.6 vol% CO_2) conditions using a two-tier flask system (Yu *et al.*, 2017). The pH of the culture under HC conditions ranged from 7.17 to 7.65, and from 7.87 to 9.96 under AC conditions. Analysis of the doubling times of all cell lines indicated that the cells generally grow faster under HC conditions. Under AC, the PEPC2 and PEPC1/2 double knockout mutants grow slower than WT, while the PEPC1 knockout mutants were not affected (Fig. 4a). The increased maximum doubling times of PEPC2 and the double knockout mutants are shown in Fig. 4(b). However, both PEPC2 and PEPC1/2 knockout mutants grew as fast as WT cells under HC conditions. The maximum doubling times of PEPC2 and PEPC1/2 knockout mutants were not different under HC conditions, but cultures need a longer time to initiate growth than WT cells. This indicates that HC conditions may compensate for the slower growth of these knockout mutants. In order to investigate whether photosynthesis is impaired by the knockout of the PEPCs, we further examined the maximum PSII quantum yield (F_v/F_m) in WT and PEPC knockout mutants under ambient air conditions. While no PEPC1 knockout mutants showed any differences in F_v/F_m compared to WT, the PEPC2 and the double-knockout mutants have slightly but significantly lower F_v/F_m values under AC conditions compared to WT (Fig. 4c).

Knocking out PEPC2 in *Phaeodactylum tricornutum* leads to reduced photosynthetic O_2 evolution under low dissolved inorganic carbon concentrations

The photosynthetic O_2 evolution of *P. tricornutum* WT and PEPC knockout mutant cells grown under AC or UHC conditions was determined in a medium of pH 8.2. The DIC concentration that results in the half maximum rate of photosynthesis ($K_{0.5}$ [DIC]) in the cells pre-cultivated under UHC conditions was > 5 times higher than in the cells grown under AC conditions (Table 1). Grown under AC conditions, the maximum rate of net photosynthesis (P_{max}) of all PEPC knockout cell lines supplied with saturating CO_2 concentrations (*c.* 660 μM) was not affected compared to WT (Fig. 5; Table 1). However, strains PEPC2-6, PEPC2-13, and PEPC1/2-7 showed significantly reduced photosynthetic O_2 evolution compared to WT when supplied with AC concentrations from 29 to 381 μM (Fig. 5; Table S6). More precisely, when the DIC concentration in the chamber was 29 μM, the corresponding photosynthetic O_2 evolution was reduced by 34% in PEPC2-6, by 37% in PEPC2-13, and by 44% in PEPC1/2-7 (Table S6). This results in a significantly increased $K_{0.5}$ [DIC] in the PEPC2-13 and PEPC1/2-7 mutants (Table 1). In contrast to these findings, no significant differences in these photosynthetic parameters were observed in PEPC1 knockout mutants grown under AC conditions (Fig. 5; Table 1).

Lower $\delta^{13}C$ values in PEPC2 and PEPC1/PEPC2 double knockout mutants

In order to evaluate the role of the PEPCs in carbon fixation, we measured the $\delta^{13}C$ values for the WT and all PEPC knockout mutants grown under LC, AC, and HC conditions using an isotope ratio mass spectrometer (IRMS). Because Rubisco discriminates between the natural stable ^{13}C isotope and the more abundant ^{12}C isotope (O'Leary, 1981), and thus incorporates ^{12}C to a higher extent into organic molecules, cells using a biochemical C_4 CCM usually have a higher share of $\delta^{13}C$ than cells relying on carbon fixation by Rubisco. The $\delta^{13}C$ values of the *P. tricornutum* biomass in our experiments are dependent on the $\delta^{13}C$ value of the DIC in the medium, and the CO_2 fixation mechanism of the cells. In our experiments, DIC concentrations in the media were maintained in correspondence to reservoirs of carbonate buffers, which were connected to the culture media via the gas phase of the culture flask (Yu *et al.*, 2017). We measured

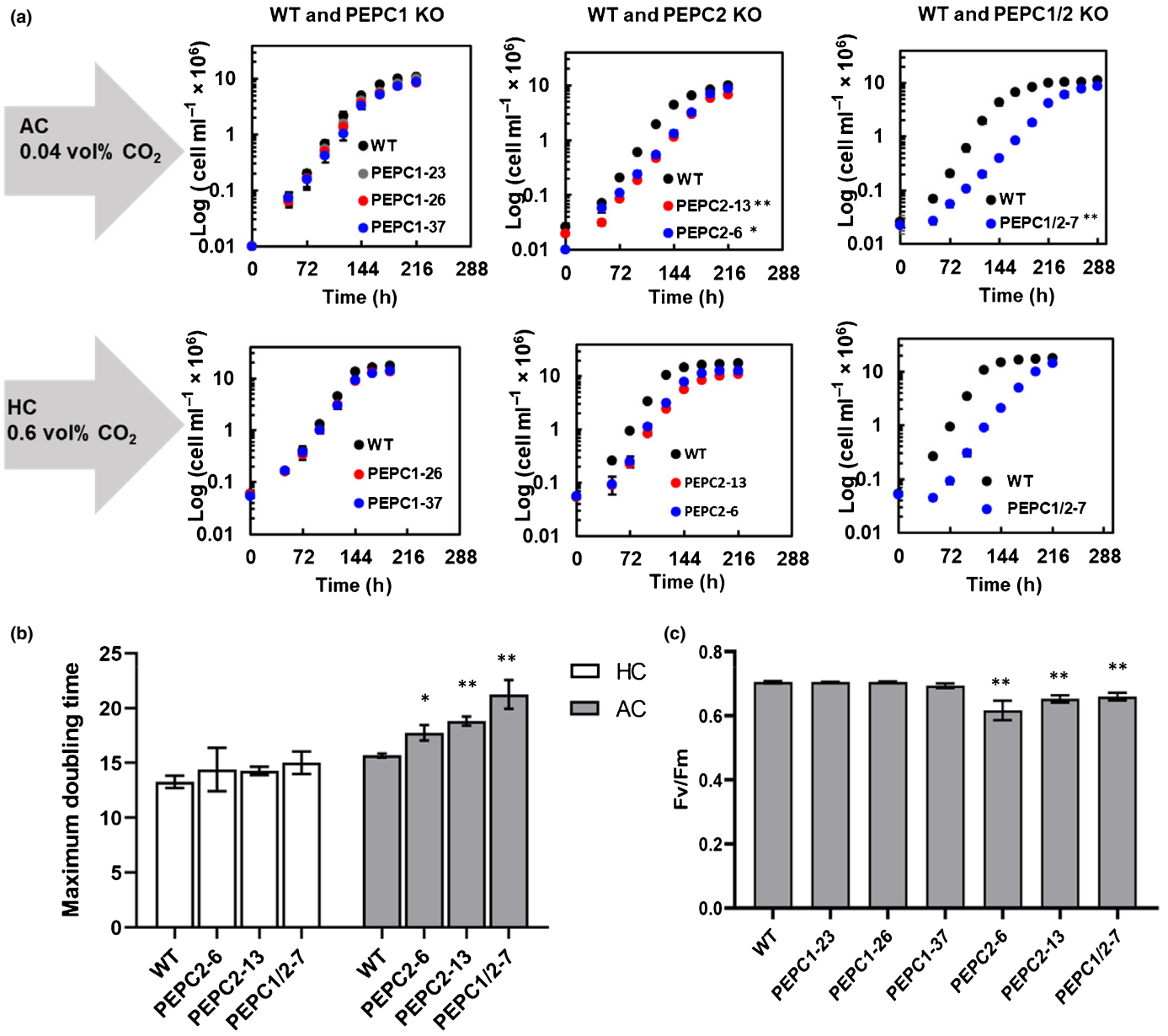

Fig. 4 (a) Growth curves of WT (wild-type) and PEPC KO (knockout) mutants of *Phaeodactylum tricornutum* under different CO_2 conditions. Cells were cultured under ambient air (AC) and 0.6 vol% CO_2 (HC). Mean ± SD of at least three independent biological replicates is shown. In all plots, filled black circles represent WT cells, and filled gray, blue and red circles represent mutants. (b) Maximum doubling time of PEPC2 and PEPC double knockout mutants. Cells were cultured under ambient air (AC) and 0.6 vol% CO_2 (HC) conditions. Mean ± SD of at least three independent biological replicates is shown. Doubling time during the exponential phase of PEPC knockout mutants and WT was calculated and compared. Student's *t*-test was used to assess statistical significance for doubling times (*, $P < 0.05$; **, $P < 0.01$). (c) Maximum photosystem II (PSII) quantum yield analyses in WT and PEPC knockout mutants grown under ambient air conditions. The PSII quantum yield was calculated as $(F_m - F_o)/F_m = F_v/F_m$. Student's *t*-test was used to assess the statistical significance of the differences between wild-type and PEPC knockout mutants (**, $P < 0.01$).

the $\delta^{13}C$ values of the $KHCO_3$ and K_2CO_3 buffer compounds used in this study (32.22‰ and −4.59‰, respectively, Table S2), which need to be seen in relation to the $\delta^{13}C$ of atmospheric CO_2 (a rough estimate of the current value would be −8.8‰, as extrapolated from the plot published in Graven *et al.*, 2017). Due to the different background $\delta^{13}C$ values of the available DIC between our experimental conditions, only the $\delta^{13}C$ values between the different strains, but grown under the same CO_2 conditions, can be compared. As expected, we observed distinct differences in the $\delta^{13}C$ values between the conditions, due to the background, with the higher CO_2 conditions having lower $\delta^{13}C$ values due to the increased contribution of the carbonate buffers to the DIC (Fig. 6). But more significantly, we also observed differences in the $\delta^{13}C$ values for the biomass of the WT and PEPC knockout strains, within the CO_2 conditions (Fig. 6). We observed that PEPC1 knockout mutants do not show any

Table 1 Photosynthetic characteristics in wild-type (WT) and phosphoenolpyruvate carboxylase (PEPC) knock-out cell lines of *Phaeodactylum tricornutum* grown under AC (ambient air) or UHC (ultra-high CO_2 1 vol %) conditions.

CO_2	Strain	pH in assay	P_{max}[1] (μmol O_2 mg^{-1} Chl h^{-1})	$K_{0.5}$ [DIC][2] (μM)
Ambient air[3]	WT	8.2	254 ± 45	29 ± 6
	PEPC1-23	8.2	241 ± 33	26 ± 10
	PEPC1-37	8.2	225 ± 8	31 ± 7
	PEPC2-6	8.2	243 ± 36	70 ± 57
	PEPC2-13	8.2	222 ± 17	50 ± 20*
	PEPC1/2-7	8.2	271 ± 21	87 ± 44*
1% CO_2[4]	WT	8.2	197 ± 21	520 ± 78
	PEPC1-23	8.2	249 ± 13*	595 ± 34
	PEPC1-37	8.2	223 ± 37	581 ± 106
	PEPC2-6	8.2	202 ± 16	449 ± 66
	PEPC2-13	8.2	140 ± 5*	399 ± 53
	PEPC1/2-7	8.2	165 ± 16*	546 ± 55

All values are mean ± SD of at least four independent biological replicates.
[1]Maximum photosynthetic rate.
[2]Dissolved inorganic carbon concentration that yields half of the maximum rate of net photosynthesis (P_{max}).
[3]Low CO_2.
[4]High CO_2.
*Student's *t*-test; $P < 0.05$.

significant differences to WT under LC, AC, or HC conditions (Fig. 6). However, PEPC2-6, PEPC2-13, and PEPC1/2-7 mutants show a significantly lower value of $\delta^{13}C$ under HC conditions (0.6 vol% CO_2); PEPC2-13 also shows a lower value of $\delta^{13}C$ under LC and AC conditions (Fig. 6). These results indicate that PEPC2 plays a role in CO_2 prefixation.

Discussion

It has been debated for a long time whether there is a C_4-like photosynthetic pathway in diatoms (Beardall *et al.*, 1976; Reinfelder *et al.*, 2000, 2004; McGinn & Morel, 2008; Kustka *et al.*, 2014). While the genes for enzymes required for such a pathway were identified more than a decade ago in the model diatoms *P. tricornutum* and *T. pseudonana* (Kroth *et al.*, 2008), their intracellular locations argue against the involvement of the enzymes in a biochemical CCM (Tanaka *et al.*, 2014; Ewe *et al.*, 2018). Also, molecular, biochemical, or physiological proof or disproof of their role in carbon fixation is scarce and in many cases is ambiguous (Roberts *et al.*, 2007; Haimovich-Dayan *et al.*, 2013; Kustka *et al.*, 2014; Clement *et al.*, 2016; Hopkinson *et al.*, 2016; Kikutani *et al.*, 2016; Matsuda *et al.*, 2017; Shen *et al.*, 2017; Ewe *et al.*, 2018; Beardall & Raven, 2020; Launay *et al.*, 2020).

Biophysical CCMs mainly rely on the enzymatic conversion of HCO_3^- and CO_2 as well as the transmembrane transport of HCO_3^-, while a biochemical CCM includes a first carbon fixation step by an enzyme other than Rubisco (Tsuji *et al.*, 2017). In contrast to Rubisco, PEPC uses HCO_3^- as a substrate for carboxylation, producing oxaloacetate (OAA), which then is transported into the chloroplast, where it can be converted to malate by a plastidic MDH. The malate then can be decarboxylated,

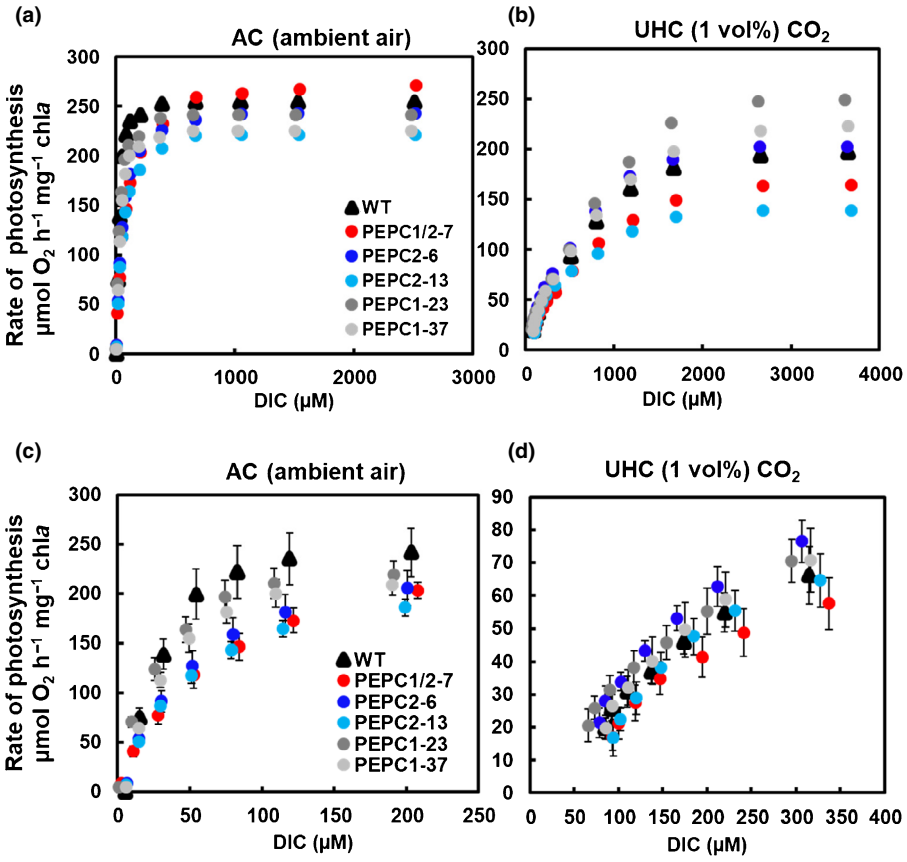

Fig. 5 Kinetic plots of photosynthetic rates in wild-type (WT) and phosphoenolpyruvate carboxylase (PEPC) knockout mutants of *Phaeodactylum tricornutum*. Cells were cultured under AC (ambient air) (a, c) or UHC (1 vol%) conditions (b, d). Their photosynthetic responses at higher DIC (dissolved inorganic carbon) concentrations (a, b) and lower DIC concentrations (c, d) are shown. Data represent mean ± SD of at least four independent biological replicates. In all plots, filled black triangles represent the WT and filled coloured circles represent PEPC knockout mutants.

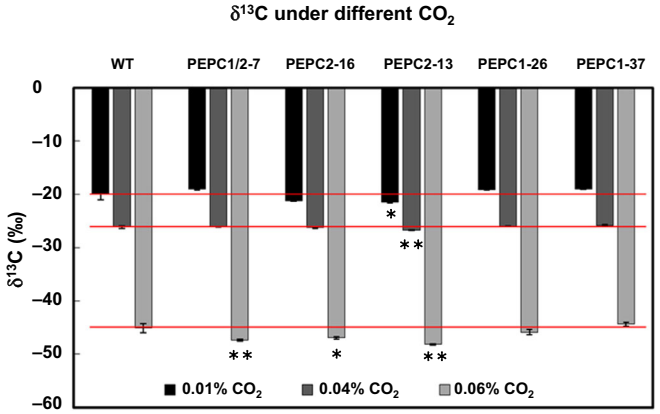

Fig. 6 Carbon stable isotope (^{13}C) signatures of wild-type (WT) and phosphoenolpyruvate carboxylase (PEPC) knockout cell lines of *Phaeodactylum tricornutum*. All cultures were grown under very low CO_2 (0.01 vol% CO_2), pseudo ambient air (0.04 vol% CO_2) and high CO_2 (0.6 vol% CO_2) conditions in two-tier vessels according to a method described previously (Yu *et al*., 2017). The $\delta^{13}C$ value of the examined *P. tricornutum* cells are at *c*. −20‰, −26‰ and −46‰, under the 0.01%, 0.04% and 0.6 vol% CO_2 conditions respectively, reflecting differences in the composition of the carbon sources (HCO_3^-/CO_3^{2-} buffers mixed at different ratios). $\Delta^{13}C$ values were calculated using Pee Dee Belemnite (PDB) as an internal standard. Error bars represent SEs of means from at least three independent biological replicates. Asterisks indicate significant differences according to Student's *t*-test (*, $P < 0.05$; **, $P < 0.01$). The red line indicates the average value for the WT.

releasing CO_2 in close proximity to Rubisco, which reduces its oxygenase activity. The generated pyruvate is then converted into PEP, which can return back to the cytosol as the substrate for PEPC (Bowes, 2010). Similarly, a single-cell C_4 pathway could also be present in diatoms and function in two different compartments of a single cell, as described in our model (see Fig. 7).

PEPC mRNA levels, protein amounts, and enzymatic activity were analyzed in WT *P. tricornutum* cells under different CO_2 concentrations. Consistent with McGinn & Morel (2008), we could not detect any changes in *PEPC* transcript levels in response to LC or HC conditions. Accordingly, different CO_2 concentrations during cultivation also had no significant effect on the total amount of PEPC protein and total PEPC enzymatic activity, indicating a constitutive expression and activity of PEPCs under different CO_2 conditions in *P. tricornutum*, which reflects the findings of some previous studies (Clement *et al*., 2016, 2017). Also, a survey among different phytoplankton groups did not show CO_2-based responses in *PEPC* transcription (Hennon *et al*., 2017), and in meta-transcriptomes sampled from marine habitats, transcripts of various C_4 enzymes did not co-occur in their individual profiles (Karlusich *et al*., 2021).

For most land plant PEPCs, the PEP substrate saturation curves follow Michaelis–Menten kinetics, including the C_3 and C_4 PEPCs of *Zea mays*. However, the photosynthetic PEPCs (besides the PEPCs of the genera *Flaveria* and *Alternanthera*) all show a sigmoidal saturation curve for the substrate PEP, indicating a cooperative PEP binding. After being activated by glucose-6-phosphate, the cooperativity disappears and the PEP saturation curve becomes hyperbolic (Svensson *et al*., 1997; Gowik *et al*., 2006). Both recombinant PEPCs of *P. tricornutum* show a sigmoidal saturation curve with PEP as substrate, indicating a cooperative PEP binding, and thus a similar enzymatic process. In general, C_4 PEPCs have shown a lower affinity for PEP than the nonphotosynthetic PEPCs (Dong *et al*., 1998; Gowik *et al*., 2006; Lara *et al*., 2006), but a higher affinity for HCO_3^- than C_3 PEPCs in land plants (Gutierrez *et al*., 1974). The recombinant PEPC2 of *P. tricornutum* has a lower affinity for PEP, but a much higher affinity for HCO_3^-, thus PEPC2 shows similar kinetic properties to C_4 PEPCs from land plants. In contrast, PEPC1 from *P. tricornutum* in this study showed a similar affinity for substrates PEP and HCO_3^-. The results indicate that the mitochondrial diatom PEPC2 may have the properties of photosynthetic PEPCs, while the plastidic PEPC1 seems to be functionally similar to nonphotosynthetic PEPCs. As both enzymes show a similar specific activity as well as similar affinities for the antiserum (Fig. 1b), this might indicate a diatom-specific post-translational modification of the enzymes.

One important tool for understanding the role of the two PEPCs in *P. tricornutum* cells is the use of PEPC knockout mutants. The reduced growth rate of PEPC2 and the double-knockout cells during incubation under LC conditions, as well as the reduced O_2 evolution when supplied with low DIC concentrations, in combination with unaffected P_{max} values when supplied with saturating DIC concentrations, indicate that knocking out PEPC2 may affect CO_2 assimilation. Photosynthetic organisms use both $^{12}CO_2$ and $^{13}CO_2$ during CO_2 fixation. PEPC does not discriminate between $^{13}CO_2$ and $^{12}CO_2$ to the same extent as Rubisco, and C_3 and C_4 plants can therefore be distinguished by their stable carbon isotope ratios (O'Leary, 1981). Accordingly, the observation that less ^{13}C is present in PEPC2 and double-knockout mutants compared to WT (Fig. 6) indicates that PEPC2-mediated carbon prefixation may occur in *P. tricornutum*. As PEPC2 activity is absent in PEPC2 and double-knockout mutants, no prefixation of $^{13}CO_2$ via PEPC2 is possible in these mutants. Interestingly, under HC conditions, we still observed less $^{13}CO_2$ fixation in PEPC2 and double-knockout mutants compared to WT, indicating that PEPC2-mediated carboxylation is also active under HC conditions, which is consistent with our finding that PEPC mRNA, protein, and enzyme activity are not affected by CO_2 concentrations. Also, compared to land plants, the low Rubisco content in *P. tricornutum* (2–3% of total protein; Losh *et al*., 2013) may also increase the relevance of PEPC under LC conditions. The physiological characterization of PEPC knockout mutants is summarized in Table S7.

When grown under AC conditions, the photosynthetic O_2 evolution is significantly reduced in the PEPC2 and the PEPC1/2 double-knockout mutants when supplied with low DIC concentrations during O_2 evolution measurements. We also observed a restored photosynthetic O_2 evolution in these PEPC knockout mutants after the addition of saturating DIC concentrations, which is in agreement with the findings of a study by McGinn & Morel (2008) in other diatom species. The net CO_2 fixation is blocked by the PEPC-specific inhibitor DCPC (3, 3-dichloro-2-(dihydroxyphosphinoyl-methyl)-propenoate) (Jenkins, 1987) at

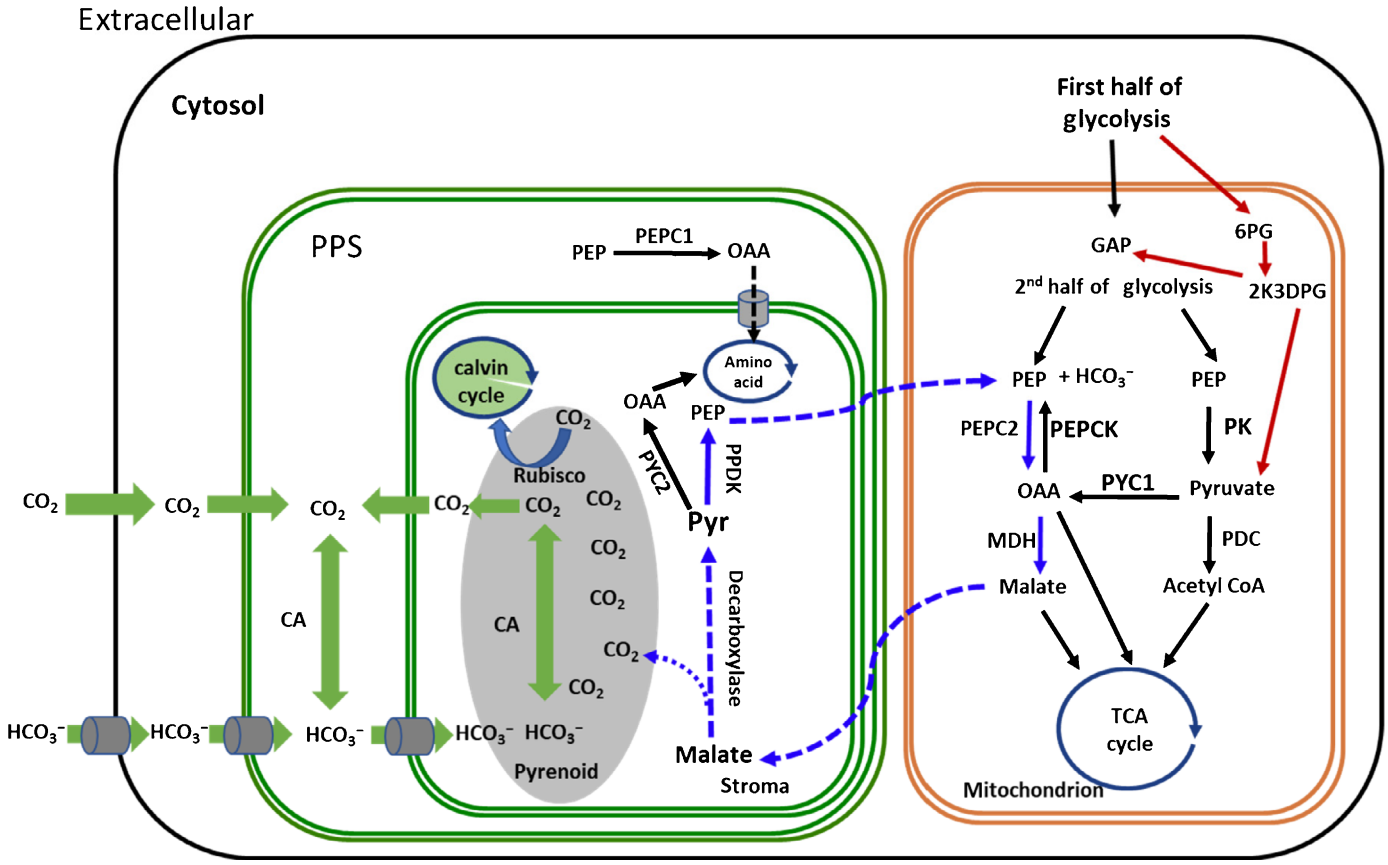

Fig. 7 Model of the biophysical CO_2 concentrating mechanism (CCM) and the proposed PEPC2 mediated C4 CO_2 concentrating mechanism (CCM) in *Phaeodactylum tricornutum*. The model of the biophysical CCM pathway is indicated by green arrows (Young & Hopkinson, 2017). The proposed C_4 pathway is marked by light blue arrows. The dashed blue arrows indicate pathways which have not yet been verified by experiments. Green lines represent the four plastid membranes, orange lines represent mitochondria with two membranes, and the black line indicates the cytoplasmic membrane. Red arrows indicate the Entner–Doudoroff pathway. 2K3DPG, 2-keto-3-deoxyphosphogluconate; 6PG, 6-phospho-gluconate; CA, carbonic anhydrase; GAP, glyceraldehyde-3-phosphate; MDH, malate dehydrogenase; ME, malic enzyme; OAA, oxaloacetate; PDC, pyruvate dehydrogenase complex; PEP, phosphoenolpyruvate; PEPC, phosphoenolpyruvate carboxylase; PEPCK, phosphoenolpyruvate carboxykinase; PPDK, pyruvate-phosphate dikinase; PPS, periplastidic space; PK, pyruvate kinase; PYC, pyruvate carboxylase.

400 μM DIC in *T. pseudonana* and *T. weissflogii*, but was restored to 50% and 80%, respectively, after adding $KHCO_3$ (McGinn & Morel, 2008). Reinfelder *et al.* (2004) also observed that *T. weissflogii* photosynthesis, after DCDP treatment, can be restored by elevated CO_2 concentrations (Reinfelder *et al.*, 2004). Complete inhibition of the PEPC activity in *P. tricornutum* by knocking out PEPCs reduces photosynthetic O_2 evolution under low DIC concentrations by only *c.* 40%. This rather small reduction in photosynthesis in *P. tricornutum* may indicate that PEPC2-mediated biochemical carbon pre-fixation only contributes to a small proportion to the total carbon fixation. The involvement of PEPC2 in carbon fixation is still surprising, considering that PEPC2 is located in the mitochondria, whereas the carboxylation by PEPC in C_4 plants occurs in the cytosol. Based on our results, we propose that the following pathways are involved in PEPC2-mediated C_4 photosynthesis in *P. tricornutum* (Fig. 7): HCO_3^- is prefixed by PEPC2 in the mitochondrion to form OAA, which can be converted into malate, which can be exported. Flori *et al.* (2017) observed physical contact between mitochondria and chloroplasts in *P. tricornutum* using focused ion beam scanning electron microscopy (FIB-SEM). This and the existence of genes encoding malate shuttle transporters (Prihoda *et al.*, 2012), may allow the energetic exchange between these two organelles (Bailleul *et al.*, 2015). Thus, we propose that malate produced in the mitochondria might be transported into the plastid via malate shuttle transporters or through physical interactions between the two organelles. Within the plastid stroma, the malate could be decarboxylated by a so-far unknown plastidic decarboxylating enzyme. One reason why the knockout of PEPC2 may only have a small effect on carbon fixation in *P. tricornutum* could be the activity of the pyruvate carboxylase PYC1 in the mitochondria, which may supply C_4 compounds as well (Ewe *et al.*, 2018). Interestingly, both enzymes could benefit from refixation of CO_2 released by the tricarboxylic acid (TCA) cycle.

Somewhat problematic for this model, though, is the lack of proof of an OAA decarboxylating enzyme in diatom plastids (Tanaka *et al.*, 2014; Ewe *et al.*, 2018). The only annotated decarboxylating enzymes in *P. tricornutum*, malic enzyme (ME) and PEPCK, have been shown to be located in mitochondria

(Ewe *et al.*, 2018), although we cannot exclude the possibility that there might be unknown enzymes in the plastids to perform a decarboxylation of malate. Revisiting the protein sequences of decarboxylating enzymes of *P. tricornutum*, we found that one of the ME isoforms (ME2) (JGI protein ID 27477) is predicted to be targeted to either mitochondria or the periplastidic space. This enzyme has also been classified as a dual targeted decarboxylase by Smith *et al.* (2012). Kustka *et al.* (2014) further suggested that the plastidic pyruvate carboxylase (PYC), in a reverse reaction to its regular function, could decarboxylate C4 acids. That assumption, though, is based on the decarboxylating activity of PYC isolated from chicken liver (Attwood & Cleland, 1986), and not on experimental evidence from diatoms. Pyruvate generated by decarboxylation of malate in plastids could be converted into PEP by PPDK, and could be transported back to the mitochondria as a substrate for PEPC2 via the malate shuttle transporters and the physical interactions between mitochondria and chloroplasts. The regeneration of PEP from pyruvate by the PPDK would be required to keep this potential C_4 cycle going. However, a report on a PPDK silencing mutant of *P. tricornutum* by Haimovich-Dayan *et al.* (2013) indicates that PPDK inhibition has little effect on photosynthesis. It is possible that the silencing effect on PPDK may not be sufficient to affect a C_4 pathway. Finally, the mitochondrial PYC1 could also supply OAA for this C_4 pathway, as it converts pyruvate to OAA (Fig. 7).

PEPC1 in *P. tricornutum* is located in the periplastidic compartment (Ewe *et al.*, 2018). Interestingly, we could not find any evidence that PEPC1 might be involved in CO_2 fixation, which raises the question of why this enzyme is targeted to this compartment. Although several proteins have been demonstrated to be located in the PPS, the role of this compartment is still unknown (Gruber & Kroth, 2017). In earlier articles, it was proposed that this compartment is acidic, eventually playing a role in concentrating CO_2 (Lee & Kugrens, 1998), but this has not yet been experimentally proven. Another possible role of PEPC1 could be the generation of carbon skeletons for amino acid synthesis. In Arabidopsis, PEPCs localized in the cytosol play a role in amino acid synthesis. Oxaloacetate produced by PEPC enters the TCA cycle, and the α-ketoglutarate generated from the TCA cycle then can be used as a precursor of glutamate synthesis in the chloroplast (Taylor *et al.*, 2010). The periplastidic PEPC1 in *P. tricornutum* could fulfill a similar function to the cytosol PEPC in Arabidopsis. The OAA produced by PEPC1 might be converted into α-ketoglutarate by the aspartate aminotransferase 4 (AAT4, JGI Protein ID 22909), which is predicted to be localized in the chloroplast (Ewe, 2015). The α-ketoglutarate would then be a substrate for the glutamate synthase (Taylor *et al.*, 2010).

Our results show that a certain proportion of the primary carbon fixation in *P. tricornutum* could be achieved by the mitochondrial PEPC2 enzyme. The contribution of this C_4-type carbon fixation to biomass formation is higher at low DIC concentrations compared to normal (in the range of air-saturated growth medium) DIC concentrations. We hypothesize that mitochondrial PEPC acts as a component of a biochemical CCM pathway in *P. tricornutum*; however, a plastidic decarboxylase would be needed for such a pathway. Reverse genetic tools like the gene knockouts used in this study will also be helpful in the future to further characterize the putative C_4-like carbon fixation in *P. tricornutum*, or other nonmodel diatoms.

Acknowledgements

This work was supported by the University of Konstanz, the Graduate School Biological Sciences (GBS) and the China Scholarship Council (CSC), as well as by JSPS Kakenhi Kiban Research (A) (grant no. 19H01153 to YM) and by JST CREST 'Cell dynamics' (grant no. JPMJCR20E1 to YM). The authors would like to thank D. Ballert (University of Konstanz) for the genetic transformation of *P. tricornutum* and the cultivation of the transformed cell lines, and Dr. Dietmar Funck for providing advice regarding protein purification. We thank Dr. Dirk Oehler for the support in constructing the phylogenetic tree.

Author contributions

GY, KN, AG, CRB, BL, YM, and PGK planned and designed the research. GY, KN, AFS, and EY performed experiments. GY, KN, AG, CRB, BL, YM, and PGK analyzed the data. GY, KN, AG, BL, YM, and PGK wrote the manuscript.

ORCID

Ansgar Gruber https://orcid.org/0000-0002-5876-4391
Peter G. Kroth https://orcid.org/0000-0003-4734-8955
Bernard Lepetit https://orcid.org/0000-0001-9980-9210
Yusuke Matsuda https://orcid.org/0000-0002-1892-4397
Kensuke Nakajima https://orcid.org/0000-0002-6134-6676
Carolina Rio Bartulos https://orcid.org/0000-0003-1203-127X
Alexander F. Schober https://orcid.org/0000-0002-5858-9407
Guilan Yu https://orcid.org/0000-0001-9251-8146

Data availability

The data that support the findings of this study are available in the Supporting Information that accompanies this article.

References

Andersson I, Backlund A. 2008. Structure and function of Rubisco. *Plant Physiology Biochemistry* **46**: 275–291.

Armbrust EV, Berges JA, Bowler C, Green BR, Martinez D, Putnam NH, Zhou S, Allen AE, Apt KE, Bechner M *et al.* 2004. The genome of the diatom *Thalassiosira pseudonana*: ecology, evolution, and metabolism. *Science* **306**: 79–86.

Ascencio J, Bowes G. 1983. Phosphoenolpyruvate carboxylase in *Hydrilla* plants with varying CO_2 compensation points. *Photosynthesis Research* **4**: 151–170.

Attwood PV, Cleland W. 1986. Decarboxylation of oxalacetate by pyruvate carboxylase. *Biochemistry* **25**: 8191–8196.

Badger MR, Andrews TJ, Whitney S, Ludwig M, Yellowlees DC, Leggat W, Price GD. 1998. The diversity and coevolution of Rubisco, plastids, pyrenoids, and chloroplast-based CO_2-concentrating mechanisms in algae. *Canadian Journal of Botany* **76**: 1052–1071.

Bailleul B, Berne N, Murik O, Petroutsos D, Prihoda J, Tanaka A, Villanova V, Bligny R, Flori S, Falconet D *et al.* 2015. Energetic coupling between plastids and mitochondria drives CO_2 assimilation in diatoms. *Nature* **524**: 366–369.

Beardall J, Mukerji D, Glover H, Morris I. 1976. The path of carbon in photosynthesis by marine phytoplankton. *Journal of Phycology* **12**: 409–417.

Beardall J, Raven JA. 2020. Acquisition of inorganic carbon by microalgae and cyanobacteria. In: Wang Q, ed. *Microbial photosynthesis*. Singapore City, Singapore: Springer, 151–168.

Besnard G, Pinçon G, D'Hont A, Hoarau J-Y, Cadet F, Offmann B. 2003. Characterisation of the phosphoenolpyruvate carboxylase gene family in sugarcane (*Saccharum* spp.). *Theoretical and Applied Genetics* **107**: 470–478.

Birmingham BC, Colman B. 1979. Measurement of carbon dioxide compensation points of freshwater algae. *Plant Physiology* **64**: 892–895.

Bowes G. 2010. Single-cell C_4 photosynthesis in aquatic plants. In: Raghavendra A, Sage R, eds. *C_4 photosynthesis and related CO_2 concentrating mechanisms, In: Advances in photosynthesis and respiration*. Dordrecht, the Netherlands: Springer, 63–80.

Bowler C, Allen AE, Badger JH, Grimwood J, Jabbari K, Kuo A, Maheswari U, Martens C, Maumus F, Otillar RP *et al.* 2008. The *Phaeodactylum* genome reveals the evolutionary history of diatom genomes. *Nature* **456**: 239–244.

Bradford MM. 1976. A rapid and sensitive method for the quantitation of microgram quantities of protein utilizing the principle of protein-dye binding. *Analytical Biochemistry* **72**: 248–254.

Burkhardt S, Amoroso G, Riebesell U, Sültemeyer D. 2001. CO_2 and HCO_3^- uptake in marine diatoms acclimated to different CO_2 concentrations. *Limnology and Oceanography* **46**: 1378–1391.

Chang KS, Jeon H, Seo S, Lee Y, Jin E. 2014. Improvement of the phosphoenolpyruvate carboxylase activity of *Phaeodactylum tricornutum* PEPCase 1 through protein engineering. *Enzyme and Microbial Technology* **60**: 64–71.

Clement R, Dimnet L, Maberly SC, Gontero B. 2016. The nature of the CO_2-concentrating mechanisms in a marine diatom, *Thalassiosira pseudonana*. *New Phytologist* **209**: 1417–1427.

Clement R, Jensen E, Prioretti L, Maberly SC, Gontero B. 2017. Diversity of CO_2-concentrating mechanisms and responses to CO_2 concentration in marine and freshwater diatoms. *Journal of Experimental Botany* **68**: 3925–3935.

Colman B, Rotatore C. 1995. Photosynthetic inorganic carbon uptake and accumulation in two marine diatoms. *Plant, Cell & Environment* **18**: 919–924.

Dong L-Y, Masuda T, Kawamura T, Hata S, Izui K. 1998. Cloning, expression, and characterization of a root-form phosphoenolpyruvate carboxylase from *Zea mays*: comparison with the C_4-form enzyme. *Plant and Cell Physiology* **39**: 865–873.

Doyle EL, Booher NJ, Standage DS, Voytas DF, Brendel VP, VanDyk JK, Bogdanove AJ. 2012. TAL Effector Nucleotide Targeter (TALE-NT) 2.0: tools for TAL effector design and target prediction. *Nucleic Acids Research* **40**: W117–W122.

Edwards GE, Franceschi VR, Voznesenskaya EV. 2004. Single-cell C_4 photosynthesis versus the dual-cell (Kranz) paradigm. *Annual Review of Plant Biology* **55**: 173–196.

Ewe D. 2015. *Living well with a scrambled metabolism: CO_2 fixation and carbohydrate pathways in the diatom Phaeodactylum tricornutum*. PhD thesis, Konstanz University, Konstanz, Germany.

Ewe D, Tachibana M, Kikutani S, Gruber A, Bártulos CR, Konert G, Kaplan A, Matsuda Y, Kroth PG. 2018. The intracellular distribution of inorganic carbon fixing enzymes does not support the presence of a C_4 pathway in the diatom *Phaeodactylum tricornutum*. *Photosynthesis Research* **137**: 263–280.

Falkowski P, Raven J. 1997. An introduction to photosynthesis in aquatic systems. In: *Aquatic photosynthesis*. Malden, MA, USA: Blackwell Science, 1–32.

Flori S, Jouneau PH, Bailleul B, Gallet B, Estrozi LF, Moriscot C, Bastien O, Eicke S, Schober A, Bártulos CR *et al.* 2017. Plastid thylakoid architecture optimizes photosynthesis in diatoms. *Nature Communications* **20**: 15885.

Giordano M, Beardall J, Raven JA. 2005. CO_2 concentrating mechanisms in algae: mechanisms, environmental modulation, and evolution. *Annual Review of Plant Biology* **56**: 99–131.

Gowik U, Engelmann S, Bläsing O, Raghavendra AS, Westhoff P. 2006. Evolution of C_4 phosphoenolpyruvate carboxylase in the genus *Alternanthera*: gene families and the enzymatic characteristics of the C_4 isozyme and its orthologues in C_3 and C_3/C_4 *Alternantheras*. *Planta* **223**: 359–368.

Graven H, Allison CE, Etheridge DM, Hammer S, Keeling RF, Levin I, Meijer HAJ, Rubino M, Tans PP, Trudinger CM *et al.* 2017. Compiled records of carbon isotopes in atmospheric CO_2 for historical simulations in CMIP6. *Geoscientific Model Development* **10**: 4405–4417.

Gruber A, Kroth PG. 2017. Intracellular metabolic pathway distribution in diatoms and tools for genome-enabled experimental diatom research. *Philosophical Transactions of the Royal Society B* **372**: 20160402.

Guillard RR. 1975. Culture of phytoplankton for feeding marine invertebrates. In: Smith ML, Chanley MH, eds. *Culture of marine invertebrate animals*. New York, NY, USA: Plenum Press, 29–60.

Guillard RR, Ryther JH. 1962. Studies of marine planktonic diatoms: I. *Cyclotella Nana* Hustedt, and *Detonula Confervacea* (CLEVE) Gran. *Canadian Journal of Microbiology* **8**: 229–239.

Gutierrez M, Gracen V, Edwards G. 1974. Biochemical and cytological relationships in C_4 plants. *Planta* **119**: 279–300.

Haimovich-Dayan M, Garfinkel N, Ewe D, Marcus Y, Gruber A, Wagner H, Kroth PG, Kaplan A. 2013. The role of C_4 metabolism in the marine diatom *Phaeodactylum tricornutum*. *New Phytologist* **197**: 177–185.

Hennon GM, Hernández Limón MD, Haley ST, Juhl AR, Dyhrman ST. 2017. Diverse CO_2-induced responses in physiology and gene expression among eukaryotic phytoplankton. *Frontiers in Microbiology* **8**: 2547.

Hill AV. 1910. The possible effects of the aggregation of the molecules of haemoglobin on its dissociation curves. *Journal of Physiology* **40**: 4–7.

Hopkinson BM, Dupont CL, Allen AE, Morel FM. 2011. Efficiency of the CO_2-concentrating mechanism of diatoms. *Proceedings of the National Academy of Sciences, USA* **108**: 3830–3837.

Hopkinson BM, Dupont CL, Matsuda Y. 2016. The physiology and genetics of CO_2 concentrating mechanisms in model diatoms. *Current Opinion in Plant Biology* **31**: 51–57.

Hopkinson BM, Meile C, Shen C. 2013. Quantification of extracellular carbonic anhydrase activity in two marine diatoms and investigation of its role. *Plant Physiology* **162**: 1142–1152.

Huang W, Haferkamp I, Lepetit B, Molchanova M, Hou S, Jeblick W, Río Bártulos C, Kroth PG. 2018. Reduced vacuolar β-1,3-glucan synthesis affects carbohydrate metabolism as well as plastid homeostasis and structure in *Phaeodactylum tricornutum*. *Proceedings of the National Academy of Sciences, USA* **115**: 4791–4796.

Jeffrey SW, Humphrey GF. 1975. New spectrophotometric equations for determining chlorophylls a, b, c1 and c2 in higher plants, algae and natural phytoplankton. *Biochemie und Physiologie der Pflanzen* **167**: 191–194.

Jenkins C. 1987. 3, 3-Dichloro-2-dihydroxyphosphinoylmethyl-2-propenoate, a new, specific inhibitor of phosphoenolpyruvate carboxylase. *Biochemistry International* **14**: 219–226.

Jensen EL, Clement R, Kosta A, Maberly SC, Gontero B. 2019. A new widespread subclass of carbonic anhydrase in marine phytoplankton. *The ISME Journal* **13**: 2094–2106.

Kaplan A, Reinhold L. 1999. CO_2 concentrating mechanisms in photosynthetic microorganisms. *Annual Review of Plant Biology* **50**: 539–570.

Karlusich JJP, Bowler C, Biswas H. 2021. Carbon dioxide concentration mechanisms in natural populations of marine diatoms: insights from Tara oceans. *Frontiers in Plant Science* **12**: 659.

Kikutani S, Nakajima K, Nagasato C, Tsuji Y, Miyatake A, Matsuda Y. 2016. Thylakoid luminal θ-carbonic anhydrase critical for growth and photosynthesis in the marine diatom *Phaeodactylum tricornutum*. *Proceedings of the National Academy of Sciences, USA* **113**: 9828–9833.

Kroth P. 2002. Protein transport into secondary plastids and the evolution of primary and secondary plastids. *International Review of Cytology* **221**: 191–255.

Kroth PG, Chiovitti A, Gruber A, Martin-Jezequel V, Mock T, Parker MS, Stanley MS, Kaplan A, Caron L, Weber T *et al.* 2008. A model for carbohydrate metabolism in the diatom *Phaeodactylum tricornutum* deduced from comparative whole genome analysis. *PLoS ONE* **3**: e1426.

Kustka AB, Milligan AJ, Zheng H, New AM, Gates C, Bidle KD, Reinfelder JR. 2014. Low CO_2 results in a rearrangement of carbon metabolism to support C4 photosynthetic carbon assimilation in *Thalassiosira pseudonana*. *New Phytologist* **204**: 507–520.

Lara MV, Casati P, Andreo CS. 2002. CO_2-concentrating mechanisms in *Egeria densa*, a submersed aquatic plant. *Physiologia Plantarum* **115**: 487–495.

Lara MV, Chuong SD, Akhani H, Andreo CS, Edwards GE. 2006. Species having C_4 single-cell-type photosynthesis in the Chenopodiaceae family evolved a photosynthetic phosphoenolpyruvate carboxylase like that of Kranz-type C_4 species. *Plant Physiology* **142**: 673–684.

Launay H, Huang W, Maberly SC, Gontero B. 2020. Regulation of carbon metabolism by environmental conditions: a perspective from diatoms and other chromalveolates. *Frontiers in Plant Science* **11**: 1033.

Lee RE, Kugrens P. 1998. Hypothesis: the ecological advantage of chloroplast ER – the ability to outcompete at low dissolved CO_2 concentrations. *Protist* **149**: 341–345.

Lepetit B, Sturm S, Rogato A, Gruber A, Sachse M, Falciatore A, Kroth PG, Lavaud J. 2013. High light acclimation in the secondary plastids containing diatom *Phaeodactylum tricornutum* is triggered by the redox state of the plastoquinone pool. *Plant Physiology* **161**: 853–865.

Losh JL, Young JN, Morel FMM. 2013. Rubisco is a small fraction of total protein in marine phytoplankton. *New Phytologist* **198**: 52–58.

Maberly SC, Ball LA, Raven JA, Sültemeyer D. 2009. Inorganic carbon acquisition by chrysophytes. *Journal of Phycology* **45**: 1052–1061.

Magnin NC, Cooley BA, Reiskind JB, Bowes G. 1997. Regulation and localization of key enzymes during the induction of Kranz-less, C_4-type photosynthesis in *Hydrilla verticillata*. *Plant Physiology* **115**: 1681–1689.

Matsuda Y, Hara T, Colman B. 2001. Regulation of the induction of bicarbonate uptake by dissolved CO_2 in the marine diatom, *Phaeodactylum tricornutum*. *Plant, Cell & Environment* **24**: 611–620.

Matsuda Y, Hopkinson BM, Nakajima K, Dupont CL, Tsuji Y. 2017. Mechanisms of carbon dioxide acquisition and CO_2 sensing in marine diatoms: a gateway to carbon metabolism. *Philosophical Transactions of the Royal Society B: Biological Sciences* **372**: 20160403.

McGinn PJ, Morel FM. 2008. Expression and inhibition of the carboxylating and decarboxylating enzymes in the photosynthetic C_4 pathway of marine diatoms. *Plant Physiology* **146**: 300–309.

Michaelis L, Menten ML. 1913. Die kinetik der invertinwirkung. *Biochemische Zeitschrift* **49**: 333–369.

Morel F, Reinfelder J, Roberts S, Chamberlain C, Lee J, Yee D. 1994. Zinc and carbon co-limitation of marine phytoplankton. *Nature* **369**: 740–742.

Morel FM, Cox EH, Kraepiel AM, Lane TW, Milligan AJ, Schaperdoth I, Reinfelder JR, Tortell PD. 2002. Acquisition of inorganic carbon by the marine diatom *Thalassiosira weissflogii*. *Functional Plant Biology* **29**: 301–308.

Nakajima K, Tanaka A, Matsuda Y. 2013. SLC4 family transporters in a marine diatom directly pump bicarbonate from seawater. *Proceedings of the National Academy of Sciences, USA* **110**: 1767–1772.

Nelson DM, Tréguer P, Brzezinski MA, Leynaert A, Quéguiner B. 1995. Production and dissolution of biogenic silica in the ocean: revised global estimates, comparison with regional data and relationship to biogenic sedimentation. *Global Biogeochemical Cycles* **9**: 359–372.

O'Leary MH. 1981. Carbon isotope fractionation in plants. *Phytochemistry* **20**: 553–567.

Prihoda J, Tanaka A, de Paula WB, Allen JF, Tirichine L, Bowler C. 2012. Chloroplast-mitochondria cross-talk in diatoms. *Journal of Experimental Botany* **63**: 1543–1557.

Rao SK, Reiskind JB, Bowes G. 2008. Kinetic analyses of recombinant isoforms of phosphoenolpyruvate carboxylase from *Hydrilla verticillata* leaves and the impact of substituting a C_4-signature serine. *Plant Science* **174**: 475–483.

Reinfelder JR. 2010. Carbon concentrating mechanisms in eukaryotic marine phytoplankton. *Annual Review of Marine Science* **3**: 291–315.

Reinfelder JR, Kraepiel AM, Morel FM. 2000. Unicellular C_4 photosynthesis in a marine diatom. *Nature* **407**: 996–999.

Reinfelder JR, Milligan AJ, Morel FM. 2004. The role of the C_4 pathway in carbon accumulation and fixation in a marine diatom. *Plant Physiology* **135**: 2106–2111.

Reiskind JB, Bowes G. 1991. The role of phosphoenolpyruvate carboxykinase in a marine macroalga with C4-like photosynthetic characteristics. *Proceedings of the National Academy of Sciences, USA* **88**: 2883–2887.

Riebesell U, Wolf-Gladrow D, Smetacek V. 1993. Carbon dioxide limitation of marine phytoplankton growth rates. *Nature* **361**: 249–251.

Roberts K, Granum E, Leegood RC, Raven JA. 2007. C_3 and C_4 pathways of photosynthetic carbon assimilation in marine diatoms are under genetic, not environmental, control. *Plant Physiology* **145**: 230–235.

Rotatore C, Colman B, Kuzma M. 1995. The active uptake of carbon dioxide by the marine diatoms *Phaeodactylum tricornutum* and *Cyclotella* sp. *Plant, Cell & Environment* **18**: 913–918.

Sage RF. 2004. The evolution of C_4 photosynthesis. *New Phytologist* **161**: 341–370.

Sage RF, Sage TL, Kocacinar F. 2012. Photorespiration and the evolution of C_4 photosynthesis. *Annual Review of Plant Biology* **63**: 19–47.

Salvucci ME, Bowes G. 1981. Induction of reduced photorespiratory activity in submersed and amphibious aquatic macrophytes. *Plant Physiology* **67**: 335–340.

Sanjana NE, Cong L, Zhou Y, Cunniff MM, Feng G, Zhang F. 2012. A transcription activator-like effector toolbox for genome engineering. *Nature Protocols* **7**: 171–192.

Serif M, Lepetit B, Weißert K, Kroth PG, Rio Bartulos CR. 2017. A fast and reliable strategy to generate TALEN-mediated gene knockouts in the diatom *Phaeodactylum tricornutum*. *Algal Research* **23**: 186–195.

Shen C, Dupont CL, Hopkinson BM. 2017. The diversity of carbon dioxide-concentrating mechanisms in marine diatoms as inferred from their genetic content. *Journal of Experimental Botany* **68**: 3937–3948.

Smith SR, Abbriano RM, Hildebrand M. 2012. Comparative analysis of diatom genomes reveals substantial differences in the organization of carbon partitioning pathways. *Algal Research* **1**: 2–16.

Svensson P, Biasing OE, Westhoff P. 1997. Evolution of the enzymatic characteristics of C_4 phosphoenol pyruvate carboxylase: a comparison of the orthologous PPCA phosphoenol pyruvate carboxylases of *Flaveria trinervia* (C_4) and *Flaveria pringlei* (C_3). *European Journal of Biochemistry* **246**: 452–460.

Tanaka R, Kikutani S, Mahardika A, Matsuda Y. 2014. Localization of enzymes relating to C_4 organic acid metabolisms in the marine diatom, *Thalassiosira pseudonana*. *Photosynthesis Research* **121**: 251–263.

Taylor L, Nunes-Nesi A, Parsley K, Leiss A, Leach G, Coates S, Wingler A, Fernie AR, Hibberd JM. 2010. Cytosolic pyruvate,orthophosphate dikinase functions in nitrogen remobilization during leaf senescence and limits individual seed growth and nitrogen content. *The Plant Journal* **62**: 641–652.

Tsuji Y, Kusi-Appiah G, Kozai N, Fukuda Y, Yamano T, Fukuzawa H. 2021. Characterization of a CO_2-concentrating mechanism with low sodium dependency in the centric diatom *Chaetoceros gracilis*. *Marine Biotechnology* **23**: 456–462.

Tsuji Y, Mahardika A, Matsuda Y. 2017. Evolutionarily distinct strategies for the acquisition of inorganic carbon from seawater in marine diatoms. *Journal of Experimental Botany* **68**: 3949–3958.

Voznesenskaya EV, Franceschi VR, Kiirats O, Artyusheva EG, Freitag H, Edwards GE. 2002. Proof of C_4 photosynthesis without Kranz anatomy in *Bienertia cycloptera* (Chenopodiaceae). *The Plant Journal* **31**: 649–662.

Whitney SM, Sharwood RE, Orr D, White SJ, Alonso H, Galmés J. 2011. Isoleucine 309 acts as a C_4 catalytic switch that increases ribulose-1,5-bisphosphate carboxylase/oxygenase (rubisco) carboxylation rate in *Flaveria*. *Proceedings of the National Academy of Sciences, USA* **108**: 14688–14693.

Young JN, Heureux AMC, Sharwood RE, Rickaby REM, Morel FMM, Whitney SM. 2016. Large variation in the Rubisco kinetics of diatoms reveals diversity among their carbon-concentrating mechanisms. *Journal of Experimental Botany* **67**: 3445–3456.

Young JN, Hopkinson BM. 2017. The potential for co-evolution of CO_2-concentrating mechanisms and rubisco in diatoms. *Journal of Experimental Botany* **68**: 3751–3762.

Yu G, Kroth PG, Gruber A. 2017. Controlled supply of CO_2 to batch cultures of the diatom *Phaeodactylum tricornutum*. *Endocytobiosis and Cell Research* **28**: 62–66.

Zaslavskaia LA, Lippmeier JC, Kroth PG, Grossman AR, Apt KE. 2000. Transformation of the diatom *Phaeodactylum tricornutum* (Bacillariophyceae) with a variety of selectable marker and reporter genes. *Journal of Phycology* **36**: 379–386.

Zhang Y, Yin L, Jiang HS, Li W, Gontero B, Maberly SC. 2014. Biochemical and biophysical CO_2 concentrating mechanisms in two species of freshwater macrophyte within the genus *Ottelia* (Hydrocharitaceae). *Photosynthesis Research* **121**: 285–297.

Zhao S, Fernald RD. 2005. Comprehensive algorithm for quantitative real-time polymerase chain reaction. *Journal of Computational Biology* **12**: 1047–1064.

Supporting Information

Additional Supporting Information may be found online in the Supporting Information section at the end of the article.

Fig. S1 Maximum likelihood analysis of phosphoenolpyruvate carboxylase sequences.

Fig. S2 Relative gene expression of bicarbonate transporters *SLC4-1*, *SLC4-2*, and *SLC4-4* in wild-type (WT) *Phaeodactylum tricornutum* cultivated at low and high CO_2 conditions.

Fig. S3 Scheme of modifications of two alleles of *PEPC1* by TALENs in PEPC1 knockout mutants.

Fig. S4 Alignment of two alleles of *PEPC1* in the WT.

Fig. S5 Alignment of *PEPC1* allele 1 between the PEPC1-23 knockout mutant and WT.

Fig. S6 Alignment of *PEPC1* between the PEPC1-37 knockout mutant and WT.

Fig. S7 Alignment of *PEPC1* in the PEPC1-26 knockout mutant (only allele 1) and WT.

Fig. S8 Alignment of *PEPC1* in the PEPC1-26 knockout mutant and WT (in the PEPC1-26 knockout mutant, allele 2 carries an 819 bp deletion).

Fig. S9 Alignment of *PEPC1* in the PEPC1-26 knockout mutant and WT (in the PEPC1-26 knockout mutant, allele 2 carries a 4 bp deletion).

Fig. S10 Alignment of *PEPC2* in the PEPC1/2-7 knockout mutant and wild-type.

Fig. S11 Scheme of amplification of different regions of the *PEPC1* gene in the PEPC1/2-7 knockout line using *PEPC1* primers.

Fig. S12 Scheme of amplification of different regions of the *PEPC2* gene in the PEPC2-6 knockout line using *PEPC2* primers.

Fig. S13 Scheme of amplification of different regions of the *PEPC2* gene in the PEPC2-13 knockout line using *PEPC2* primers.

Fig. S14 Scheme of amplification of different regions of the *PEPC2* gene in the PEPC1/2-7 knockout line using *PEPC2* primers, and scheme of modifications of allele 1 of *PEPC2* in PEPC1/2-7.

Fig. S15 Southern blots of WT and PEPC knockout mutants.

Methods S1 Supplementary materials and methods.

Table S1 Primers used in this study.

Table S2 Ratios of ^{13}C : ^{12}C ($\delta^{13}C$) for salts used for the preparation of f/2 medium and the $KHCO_3/K_2CO_3$ powders.

Table S3 Kinetic enzymatic properties of recombinant PEPCs with PEP as variable substrate; error values represent the SD of at least three independent biological replicates.

Table S4 Kinetic enzymatic properties of recombinant PEPCs with HCO_3 as variable substrate; error values represent the SD of at least three independent biological replicates.

Table S5 Summary of genetic and enzymatic characterization of PEPC knockout mutants.

Table S6 Representation of Fig. 5(c) with values.

Table S7 Summary of the physiological characterization of PEPC knockout mutants.

Please note: Wiley Blackwell are not responsible for the content or functionality of any Supporting Information supplied by the authors. Any queries (other than missing material) should be directed to the *New Phytologist* Central Office.